Research Square

Preprints are preliminary reports that have not undergone peer review.
They should not be considered conclusive, used to inform clinical practice,
or referenced by the media as validated information.

TFAP2A/AKR1B10 axis promotes clear cell renal cell carcinoma metastasis by facilitating anoikis resistance

Jihuan Yuan
Zhejiang University School of Medicine First Affiliated Hospital
Yuxiao Li
Zhejiang University School of Medicine First Affiliated Hospital
Xinyang Niu
Tsinghua University Affiliated Beijing Tsinghua Changgung Hospital: Beijing Tsinghua Changgung Hospital
Xueyou Ma
Zhejiang University School of Medicine First Affiliated Hospital
Jiazhu Sun
Zhejiang University School of Medicine First Affiliated Hospital
Fenghao Zhang
Zhejiang University School of Medicine First Affiliated Hospital
Yuchen Shi
Zhejiang University School of Medicine First Affiliated Hospital
Suyuelin Huang
Zhejiang University School of Medicine First Affiliated Hospital
kai Yu
Zhejiang University School of Medicine First Affiliated Hospital
Jiawei Zhang
Zhejiang University School of Medicine First Affiliated Hospital
Dingheng Lu
Zhejiang University School of Medicine First Affiliated Hospital
Ben Liu
drliuben@zju.edu.cn

Zhejiang University School of Medicine First Affiliated Hospital https://orcid.org/0000-0002-0709-6784

Research Article

Keywords: ccRCC, anoikis, anoikis resistance, AKR1B10, TFAP2A, metastasis

Posted Date: November 6th, 2026

DOI: https://doi.org/10.21203/rs.3.rs-11432314/v1

License: This work is licensed under a Creative Commons Attribution 4.0 International License.
Read Full License

Abstract

Background: Clear cell renal cell carcinoma (ccRCC) is characterized by a high propensity for metastasis, which critically depends on the acquisition of anoikis resistance (AR), but the molecular drivers of AR remain undefined. This study aims to elucidate the functional role and regulatory mechanisms of AKR1B10 in AR and metastatic progression in ccRCC. **Methods:** Anoikis-resistant ccRCC sublines were established using prolonged suspension culture. RNA sequencing and bioinformatic analyses identified differentially expressed genes. Clinical significance of AKR1B10 and its upstream transcription factor TFAP2A was assessed using TCGA-KIRC dataset and tissue microarrays. Biological functions of the TFAP2A/AKR1B10 axis were investigated through in vitro assays including Western blotting, qRT-PCR, flow cytometry, wound healing, and transwell migration/invasion assays. Regulatory relationship was confirmed via dual-luciferase reporter and ChIP assays. In vivo metastatic potential was evaluated using a tail-vein lung metastasis model in nude mice.

Results: AKR1B10 was identified as one of the upregulated genes in AR cells. High AKR1B10 expression was correlated with advanced TNM (Tumor-Node-Metastasis) staging, and poor prognosis in ccRCC. Functionally, AKR1B10 knockdown suppressed epithelial-mesenchymal transition (EMT), induced apoptosis, and significantly inhibited the migration, invasion, and in vivo metastatic capacity of ccRCC, while its overexpression produced the opposite effects. Mechanistically, TFAP2A was identified as a direct upstream transcription factor that binds to the AKR1B10 promoter, activating its transcription. Rescue experiments confirmed that AKR1B10 is a critical mediator of TFAP2A-driven malignant phenotypes. The oncogenic role of the TFAP2A/AKR1B10 axis was validated in both cell lines and an in vivo metastatic model.

Conclusions: The TFAP2A/AKR1B10 axis is a novel driver of AR and metastasis in ccRCC. TFAP2A upregulates AKR1B10 to promote EMT and survival of detached cells. AKR1B10 serves as a prognostic biomarker and potential therapeutic target for metastatic ccRCC.

1. Introduction

Renal cell carcinoma (RCC), the most common malignant solid tumor of the genitourinary system, constitutes about 90% of renal malignancies and approximately 3% of all cancers[1,2]. Overall, the global incidence of RCC is increasing[1]. According to global cancer statistics, the number of new RCC cases worldwide exceeded 442,570 in 2024, with approximately 144,871 related deaths during the same period[3]. China and the United States exhibit the highest incidence rates of RCC worldwide, with case counts roughly double those of Japan, which occupies the third position[4]. According to the 2024 epidemiological statistics, the number of new cases of kidney malignancies in China is approximately 0.64 times that of the United States, whereas the number of deaths is 1.07 times higher[5]. The pathogenesis of RCC involves a complex interplay of multiple factors. Rather than being determined by a single variable, the risk of RCC arises from a combination of lifestyle habits, environmental exposures,

and individual genetic susceptibility. Established risk factors include smoking, obesity, hypertension, family history, occupational exposure, and organic solvents[6].

Clear cell renal cell carcinoma (ccRCC), which originates from the proximal tubular epithelial cells of the nephron, is the most prevalent pathological subtype among all RCC variants. This subtype typically exhibits a highly heterogeneous invasive phenotype and is associated with a poor prognosis[7,8]. Approximately 40% of patients with localized ccRCC develop local recurrence or distant metastasis after surgical resection[9]. Furthermore, the insidious nature of ccRCC, coupled with a lack of specific clinical manifestations and effective diagnostic biomarkers in its early stages, means that approximately 30% of patients have already progressed to the metastatic stage at the time of initial diagnosis[10]. For patients with advanced or metastatic ccRCC, conventional chemotherapy and radiotherapy confer only limited clinical benefit[11]. Currently, the primary therapeutic armamentarium for advanced ccRCC remains centered on immune checkpoint inhibitors (ICIs) and tyrosine kinase inhibitors (TKIs)[1,10,12]. However, clinical evidence indicates that patients with advanced ccRCC frequently develop acquired resistance to TKIs within 6 to 15 months of treatment initiation[13] and patients receiving ICIs also frequently encounter disease progression during the treatment[14–16]. Therefore, an investigation into the molecular regulatory mechanisms underlying ccRCC tumorigenesis, progression, and metastasis is of particular importance for the identification of early diagnostic biomarkers and novel therapeutic targets.

Under physiological conditions, cell growth and differentiation are tightly regulated in a spatiotemporal manner, a process that depends on precise interactions between integrin receptors on the cell surface and the extracellular matrix (ECM). Once this adhesion is disrupted, cells that have detached from the ECM initiate a programmed cell death process known as anoikis[17]. As a critical mechanism for maintaining tissue homeostasis and organismal development, anoikis is recognized as a natural barrier against tumor metastasis[18,19]. However, anoikis resistance (AR) enables tumor cells to survive after detachment from the primary site and during subsequent dissemination to distant organs[20–23]. Anoikis resistance involves a spectrum of adaptive molecular alterations that collectively enhance tumor cell survival, invasiveness, therapeutic tolerance, and disease recurrence[18,22]. Accumulating evidence has demonstrated that anoikis resistance is closely associated with the progression and metastasis of various malignancies. In prostate cancer, the ATF4/CEMIP/PKCα axis has been shown to induce anoikis resistance by enhancing protective autophagy[24]. In hepatocellular carcinoma, the 14-3-3σ protein drives anoikis resistance and metastasis via activation of the EGFR-dependent ERK1/2 signaling pathway, a process achieved through the inhibition of EGFR degradation[25]. In addition, anoikis resistance has also been implicated in the metastatic progression of various other malignancies, including lung cancer[26] and breast cancer[27]. Although an association between anoikis resistance and metastatic RCC has been documented[28,29], the underlying molecular mechanisms that confer this resistance in RCC have yet to be fully elucidated. The objective of the present study is to characterize the molecular basis of anoikis resistance in ccRCC and to identify the upstream regulators governing this resistance.

2. Materials and methods

2.1 Cell culture

Both 769-P and 786-O cell lines were acquired from the Chinese Academy of Sciences Shanghai Cell Bank (Shanghai, China) and subsequently grown in RPMI 1640 medium (Hyclone, USA). The culture medium was supplemented with 10% FBS (Biologic Industries, Israel) and 1% penicillin/streptomycin (Servicebio, Wuhan, China). Regular mycoplasma detection was conducted on all cell cultures, which were incubated under humidified conditions at 37 °C with 5% CO_2.

2.2 Establishment of ccRCC cell line with anoikis resistance

Cells at the logarithmic growth phase were harvested by trypsinization and centrifugation at 1,000 rpm, then resuspended and counted. The prepared cell suspension was seeded into ultra-low attachment six-well plates (Beyotime, Shanghai, China) at a density of 1×10^5 cells per well, and the medium was replaced every 2–3 days. After 7 days of suspension culture, the cells were collected and centrifuged. The supernatant was discarded, and the cell pellet was treated with 1 mL of trypsin solution (Gibco, Hangzhou, China) for 5 minutes, followed by neutralization with 1 mL of complete medium. After gentle pipetting, the cells were centrifuged again at 1,000 rpm. The supernatant was removed, and the cell pellet was resuspended in complete medium and transferred to regular six-well adherent culture plates. Cells that re-attached and regained proliferative capacity under adherent conditions were defined as anoikis-resistant cells and were used for subsequent experiments.

2.3 Western blot

Western blot was conducted according to protocols described in a previous study[30]. Protein isolation from cell lysates was accomplished using RIPA buffer (Fude Bio, Hangzhou, China) spiked with both protease and phosphatase inhibitors (Fude Bio, Hangzhou, China). Total protein was quantified with a BCA protein assay kit (Beyotime Institute of Biotechnology, China), after which 30 μg samples were loaded for separation by SDS-PAGE and subsequent blotting onto PVDF membranes. Prior to primary antibody incubation, the membranes were blocked with 5% skim milk in Tris-buffered saline containing Tween 20 (TBST) for 1.5 h at 25°C, followed by an overnight exposure to the primary antibodies at 4°C. After three TBST washes, the membranes were exposed to HRP-conjugated secondary antibodies (1:4000, GB23301/GB23303, Servicebio, Wuhan, China) for 2h at RT. Chemiluminescent signals were captured via ECL, and β-actin was adopted as the reference protein for normalization. Supplementary Table 1 displays the utilized primary antibodies.

2.4 Quantitative real-time PCR

Total RNA extraction from cell samples, performed with RNAiso Plus Reagent (Takara) and conducted in accordance with the manufacturer's protocol, was followed by storage at −80°C, with concurrent elimination of genomic DNA contamination. Quantification of RNA concentration and purity was

subsequently accomplished using a NanoDrop 2000 spectrophotometer (Thermo Fisher Scientific). For cDNA synthesis, reverse transcription of 1-μg total RNA aliquots was achieved via the cDNA Reverse Transcription Kit (Vazyme, China), strictly adhering to the prescribed procedure. Upon completion of cDNA preparation, quantitative real-time PCR was carried out on a Bio-rad CFX96 Detection System utilizing SYBR qPCR Mix (Vazyme, China). For relative quantification, data analysis via the ΔΔCT method was performed, with β-actin serving as the normalization reference. All statistical evaluations and graphical outputs were generated using GraphPad Prism software (version 10.0). Supplementary Table 2 lists the primers for qPCR.

2.5 Plasmids Transfection

Cells were seeded into 6-well plates at a density calibrated to yield 60-70% confluence on the day of transfection, followed by incubation at 37°C in a humidified incubator with a 5% CO_2 atmosphere. 1 μg of plasmid DNA and either Lipofectamine 3000 (Thermofisher, USA) or JetPRIME transfection reagent (Polyplus, USA) were each diluted separately in the appropriate buffers as per the respective manufacturer's instructions, with Lipofectamine 3000 being prediluted prior to mixing with DNA. The resulting mixtures were then incubated at room temperature for 20 min to allow complete complex formation. Concurrently with complex formation, the original culture medium in each well was replaced with 1500 μL of fresh serum-free medium. Upon completion of the 20-min incubation, the transfection complexes were delivered dropwise to the corresponding wells, and the plate was gently agitated to achieve homogeneous distribution. The plate was then returned to the incubator for an 8 h transfection period. At the end of the transfection period, the transfection medium was aspirated and substituted with 1 mL of complete growth medium (supplemented with serum and antibiotics) per well to support subsequent cell proliferation and transgene expression. Supplementary Table 3 presents the shRNA sequences for knocking down AKR1B10 and TFAP2A.

2.6 Lentiviral construction

293T cells were plated in 6 well plates at a density of 1.0×10^6 cells/well with 2 mL of lentiviral packaging medium and incubated overnight (37 °C, 5% CO_2) to reach approximately 70% confluence. Transfection mixtures were prepared by combining 3 μg of transfer vector and 9 μg of packaging plasmids with JetPRIME reagent (Polyplus, USA) in Opti-MEM, strictly following the manufacturer’s guidelines, and incubated for 10–20 min at RT to ensure full complex formation. During this incubation, the original medium was exchanged with 1 mL of fresh packaging medium, and the DNA–lipid complexes were added dropwise to each well, followed by 24 h of culture at 37 °C in 5% CO_2. After this initial incubation, the transfection medium was removed and replaced with 2 mL of pre-warmed fresh packaging medium, with the plate returned to the incubator overnight. The first supernatant was harvested, stored at 4 °C, and the wells were refilled with another 2 mL of packaging medium. Following the second overnight collection, the two supernatant fractions were pooled and centrifuged at 2000 rpm for 10 min at RT to remove cellular debris. The cleared supernatant was then passed through a 0.45 μm filter, divided into cryovials, and preserved at –80 °C.

2.7 Establishment of stable transfection cell lines

HEK-293T cells were seeded in 6 cm culture dishes with 3 mL of DMEM complete medium and cultured at 37 °C in a cell incubator. When the cells reached 60%–70% confluence, they were co-transfected with lentiviral knockdown plasmids and the packaging plasmids pMD2.G and psPAX2. At 24 hours post-transfection, the medium was replaced, and 786-O and 769-P cells were simultaneously seeded into T25 flasks for subsequent stable knockdown or overexpression model establishment. At 48 and 72 hours post-transfection, the viral supernatant was collected using a 5-mL sterile syringe, filtered through a 0.45 μm filter, and added to the target 786-O and 769-P cells. After 48 hours of viral infection, the medium was replaced and puromycin was added to a final concentration of 2 μg/mL for selection over 48 hours. The medium was then refreshed with puromycin at 5 μg/mL for an additional 48 hours of selection. Stable transduction efficiency was verified by fluorescence microscopy and Western blotting, and the successfully transduced cell lines were obtained.

2.8 Transwell cell migration assay

Transwell migration assays were conducted using chambers (Corning, USA) following standard protocols. Cells were trypsinized and collected by centrifugation, and resuspended in serum-free medium. After gentle resuspension by pipetting to yield a single-cell population, the cells were counted and adjusted to a density of 1×10^6 cells/mL in serum-free medium. For the migration assay, 500 μL of complete medium containing 10% fetal bovine serum was added to the lower chamber, and 100 μL of the cell suspension was seeded into the upper chamber. The plates were then incubated overnight at 37°C in a cell culture incubator. After incubation, cell fixation was performed by dispensing 600 μL of pre-chilled methanol into each well, followed by a 30 min incubation on ice. The methanol was then removed, and 600 μL of 0.1% crystal violet solution was added for staining at room temperature for 20 min. The stained cells were rinsed five times with distilled water, and residual crystal violet on the upper surface of the membrane was carefully removed with a cotton swab. After complete air-drying at room temperature, the migrated cells were visualized and photographed under a microscope. All experiments were performed independently in triplicate, and the data were subjected to statistical analysis.

2.9 Transwell cell invasion assay

Matrigel (BD Biosciences, USA)was transferred from -20 °C to 4°C and allowed to thaw slowly overnight. To prevent premature gelation, pipettes, tips, microcentrifuge tubes, Transwell inserts, and serum-free medium were pre-chilled on ice. The Matrigel was diluted with pre-chilled serum-free medium at a ratio of 1:3. An aliquot of 60 μL of the diluted Matrigel was added to the upper chamber of each insert and gently spread by rocking the 24 well plate to ensure uniform coverage. The plate was then incubated at 4°C for 30 min, followed by transfer to 37°C for 2 h to allow gel polymerization. Cells were harvested by standard trypsinization and centrifugation. The cell pellet was resuspended in serum-free medium, and a single-cell suspension was obtained by gentle pipetting. After counting, the cell density was adjusted to 1×10^6 cells/mL. For the invasion assay, 500 μL of complete medium containing 10% fetal bovine serum was added to the lower chamber as a chemoattractant, and 100 μL of the cell suspension was seeded

into the upper chamber. The plates were then incubated overnight at 37°C in a cell culture incubator. The subsequent steps are in accordance with transwell cell migration assay.

2.10 Wound healing assay

Cells in six-well plates that had been transfected 48 h prior were trypsinized, neutralized with an equal volume of complete medium, and centrifuged at 1,000 rpm for 5 min to obtain cell pellets. The pellets were resuspended in 1 mL of serum-free medium. An aliquot of the cell suspension was seeded into six-well plates and cultured at 37 °C with 5% CO_2 until reaching 80%-90% confluence. A straight scratch was then gently made across the cell monolayer using a sterile 1-mL pipette tip to create a cell-free zone of uniform width. The cells were gently washed once or twice with PBS to remove detached cellular debris generated by the scratching procedure. The original medium was aspirated and replaced with fresh serum-free or low-serum medium to minimize the effects of serum-derived growth factors on cell proliferation. Immediately after scratch creation, the scratch area in each well was photographed under a microscope as the experimental baseline (0 h). Subsequent images were captured at a preset interval (24 h) to monitor the dynamic changes in wound closure.

2.11 Flow cytometry

The 10× binding buffer was diluted to a working concentration with 1×PBS (1:10 dilution) and equilibrated to room temperature. Target suspension cells were collected into centrifuge tubes and pelleted by centrifugation at 1,000 rpm. The supernatant was removed, and the cell pellet was gently resuspended in 1 mL of trypsin solution and incubated at room temperature for 5 min. Then, 1 mL of complete medium was added to neutralize the digestion, and the cells were centrifuged again at 1,000 rpm. The supernatant was discarded, and the cell pellet was resuspended in 1×PBS and washed by centrifugation; this washing step was repeated three times to thoroughly remove residual reagents. After the final wash, the supernatant was removed, and the cell pellet was resuspended in 100 μL of the working concentration of binding buffer. Subsequently, 5 μL of FITC-labeled Annexin V and 5 μL of propidium iodide (PI) were added sequentially, and the mixture was gently vortexed and incubated on ice in the dark for 15 min. Finally, 200 μL of binding buffer was added, and the stained cells were analyzed by flow cytometry within 1h.

2.12 Dual-luciferase reporter assay

293T cells were seeded into 24-well plates at a density of 1.0×10^5 cells per well. On the following day, co-transfection was performed using Lipofectamine 3000 with a mixture of the firefly luciferase reporter plasmid and the Renilla luciferase control plasmid, followed by overnight incubation at 37°C under 5% CO_2 to allow for plasmid internalization and subsequent transgene expression. Upon completion of the transfection period, the culture medium was removed, and the cells were gently rinsed with PBS before being lysed with 0.1 mL of passive lysis buffer per well. 20 μL aliquots of the resulting cell lysates were transferred in duplicate into a white opaque 96-well plate. Firefly luciferase activity was then initiated by the automated injection of 0.1 mL of LAR II reagent into each well, and after a 1-min delay, the emitted

bioluminescent signals were quantified using a microplate luminometer. Subsequently, the firefly luminescence was quenched, and Renilla luciferase activity was concurrently activated by the addition of 0.1 mL of Stop & Glo® Reagent per well, with the corresponding Renilla signals recorded immediately thereafter. The raw firefly luciferase readings were divided by the corresponding Renilla luciferase values to correct for variations in transfection efficiency and cell viability. The normalized luciferase activity from transcription-factor-treated samples was then compared against that from the empty-vector control group, and the results were expressed as fold change in transcriptional activity. The specific mutant plasmid sequences used in these dual-luciferase reporter assays are provided in Supplementary Table 4.

2.13 ChIP-qPCR

ChIP assays were conducted using a commercial ChIP kit. ccRCC cells cultured in 15 cm dishes at 80-90% confluence were gently rinsed once with ice-cold PBS, followed by the addition of 10 mL of 1% paraformaldehyde per dish and incubation on a rocking platform (50 rpm) for 10 min at room temperature to effect crosslinking. Crosslinking was then quenched by the addition of pre-chilled glycine to a final concentration of 0.125 M, with incubation continuing on the rocker for an additional 5 min. After two subsequent washes with ice-cold PBS, cell harvesting was performed by scraping, and the collected cells were transferred to 5 mL centrifuge tubes, followed by centrifugation at 500×g for 5 min at 4°C to pellet the cells. the resulting pellet was resuspended in 1 mL of pre-chilled Cell Lysis Buffer (comprising 10 mM Tris-HCl pH 8.0, 10 mM NaCl, 0.2% NP-40, and 1×protease inhibitor) and incubated on ice for 15 min. The lysate was then transferred to a sonicator and subjected to ultrasonic fragmentation using the following parameters: 40% amplitude, 30 s pulses alternating with 30-s rest intervals, for a total of 8 cycles, to generate DNA fragments ranging from 200 to 500 bp. Following sonication, a 50 µL aliquot of the lysate was reserved as the Input fraction, immediately flash-frozen in liquid nitrogen, and stored at -80°C. The remaining sample was centrifuged at 11,600×g for 10 min at 4°C to remove insoluble debris, and the clarified supernatant was transferred to a fresh tube. 5 µg of target-specific monoclonal antibody was added to the clarified supernatant, along with IP Buffer to bring the final volume to 600 µL (containing 50 mM Tris-HCl pH 8.0, 150 mM NaCl, and 1% Triton X-100). The mixture was incubated with rotation at 4°C for 4 h to allow antibody–antigen binding. Subsequently, 50 µL of pre-blocked Protein A/G magnetic beads (pre-washed three times with PBS) were introduced, and the incubation was continued with rotation overnight at 4°C. Upon completion of the overnight immunoprecipitation, the beads were subjected to sequential washing with 1 mL each of Low-Salt Wash Buffer, High-Salt Wash Buffer, LiCl Wash Buffer, and Tris-EDTA Buffer, with each wash performed under rotation at 4°C for 5 min. After the final wash, the supernatant was discarded, and the bead-bound complexes were eluted by the addition of 50 µL of Elution Buffer (100 mM $NaHCO_3$, 1% SDS) followed by incubation in a metal bath at 65°C for 15 min. The eluate was collected, and crosslink reversal was achieved by the addition of 5 µL of 5 M NaCl and incubation at 65°C for 6 h. Subsequent protein and RNA removal was accomplished by the addition of 1 µL of RNase A (10 mg/mL) and 10 µL of Proteinase K (20 mg/mL), with digestion performed at 45°C for 1 h. The purified DNA was finally recovered using a DNA purification kit, with the final elution volume adjusted to 30 µL. The subsequent steps are in accordance with qPCR.

2.14 Establishment of a Tail Vein Metastasis Model in Nude Mice

Stable knockdown cell lines were first expanded. Cells were cultured in 10 cm dishes and harvested during the logarithmic growth phase at 80%-90% confluence. The culture medium was refreshed one day prior to cell collection. The cells were trypsinized with 1.5 mL of trypsin solution; after detachment, 1.5 mL of complete medium was added to neutralize the digestion. The cell suspension was transferred to a 15 mL centrifuge tube and centrifuged at 1,000 rpm for 5 min to obtain the cell pellet. The supernatant was discarded, and the cells were washed twice with 1 mL of PBS by centrifugation. The cell pellet was resuspended in PBS and counted. Ten 4-week-old male BALB/c nude mice were randomly divided into two groups of five mice each. For tail vein injection, the lower one-third of the lateral tail vein was selected; the needle was inserted slowly and parallel to the vein. Each mouse received 100 μL of cell suspension containing 2×10^6 cells. After injection, the puncture site was gently pressed with a sterile cotton ball to achieve hemostasis. From the first day post-injection, the mice were monitored daily. At 7 days post-injection, tumor metastasis was evaluated by intraperitoneal injection of 100 μL of potassium luciferin salt, followed by bioluminescence imaging. After the tumors metastasized and grew stably, in vivo imaging was performed on each mouse, and the bioluminescent signals (fluorescence intensity) were recorded for subsequent analysis. All mice were euthanized in strict accordance with animal ethics guidelines. The lungs harboring metastatic nodules were excised, placed in sample tubes containing universal fixative, and stored at room temperature. The specimens were promptly embedded for further histological examination.

2.15 Statistical analysis

For in vitro experiments, at least three replicate wells were used per group, and all in vitro assays were independently repeated a minimum of three times. For the in vivo study, each experimental group comprised five BALB/c nude mice. Statistical analyses were performed using GraphPad Prism 10.0 and SPSS 22.0 software. All data are presented as mean±standard deviation (SD). Between-group comparisons were evaluated using two-tailed unpaired Student's t-test or non-parametric tests, as appropriate, to calculate P values. A P value of < 0.05 was considered statistically significant. Non-significant results are denoted as "ns" (not significant), while significant differences are indicated as follows: * for $p < 0.05$, ** for $p < 0.01$, and *** for $p < 0.001$.

3. Results

3.1 Establishment of an anoikis-resistant clear cell renal cell carcinoma model

We seeded the human renal clear cell carcinoma cell lines 786-O and 769-P in ultra-low adhesion six-well plates for a 7-daysuspension culture, and then transfered them to regular cell culture plates for further cultivation. The cells that adhere and proliferate stably were selected as anoikis-resistant cell, and were named 786-O-AR and 769-P-AR respectively. The parental cells that were not subjected to suspension

culture treatment were named 786-O-P and 769-P-P. The parental cells that were not subjected to suspension culture treatment are named 786-O-P and 769-P-P. To verify the effectiveness of the disintegrated apoptosis model construction, we used FITC/PI double staining combined with flow cytometry to detect the apoptosis rates of the parental cells and the disintegrated apoptosis-resistant cells that has been cultured in suspension for 48 hours. The results demonstrated that the apoptosis rates of 786-O-AR and 769-P-AR were significantly lower than those of their respective parental cells (Fig. 1A and Fig. 1B). The Western Blot experiment analysis revealed that compared with the parental cells, the protein expressions of N-Cadherin, MMP-2, Vimentin and SLUG were significantly upregulated in anoikis-resistant cells (Fig. 1C and Fig. 1D). Meanwhile, the anti-apoptotic proteins Mcl-1 and Bcl-2 were also highly expressed in anoikis-resistant cells, while the expression of the pro-apoptotic protein Bax was significantly reduced (Fig. 1C and Fig. 1D). Consistently, we employed transwell cell migration/invasion assay (Fig. 1E and Fig. 1F) and wound healing assay (Fig. 1G and Fig. 1H) to investigate the effect on the invasion and migration abilities of anoikis-resistant ccRCC. The results showed that compared with the parental cells, the number of anoikis-resistant cells passing through the polycarbonate membrane and Matrigel matrix gel was significantly increased, and the anoikis-resistant cells exhibited stronger migration ability. In conclusion, we successfully established the anoikis-resistant cell model of 786-O and 769-P, which possessed stronger anti-apoptotic, invasive and migratory capabilities.

3.2 AKR1B10 is highly expressed in metastatic ccRCC and is associated with poor prognosis.

To explore the molecular mechanism underlying the anoikis-resistance of ccRCC, we conducted RNA sequencing on 786-O-P and 786-O-AR cells and screened for differentially expressed genes. According to the volcano plot, the expression level of AKR1B10 was significantly elevated in anoikis-resistant ccRCC cells, displaying a fold change of 2.019 (log2 FC = 1.014, adj.P = 0.002) (Fig. 2A). The GO functional enrichment analysis revealed that the differentially expressed genes were mainly enriched in biological processes such as cell adhesion, extrinsic apoptotic pathways, and laminin binding (Fig. 2B). To further clarify the clinical significance of AKR1B10 in ccRCC, we analyzed the correlation between its expression level and the prognosis of patients, as well as its correlation with tumor stage in TCGA-KIRC database. The results demonstrated that the expression of AKR1B10 in tumor tissues of patients with T3/T4 stage ccRCC was significantly higher than that in patients with T1/T2 stage (Fig. 2C). Moreover, patients with lymph node metastasis (N1) and distant metastasis (M1) also exhibited higher expression levels (Fig. 2C). In addition, patients with high expression of AKR1B10 in ccRCC had poorer overall survival (OS), disease-specific survival (DSS), and progression-free interval (PFI) (Fig. 2D). These findings suggested that AKR1B10 was overexpressed in metastasis ccRCC and was closely associated with the metastatic potential and poor prognosis of ccRCC.

We further detected the expression level of AKR1B10 in ccRCC to validate the results of the bioinformatics analysis. Western blot and qPCR analyses were performed in AR cell and their parental

cell lines. The results demonstrated that the mRNA and protein levels of AKR1B10 were relatively elevated in the 786-O-AR and 769-P-AR cell lines (Fig. 2E-G). In addition, we also investigated the expression of AKR1B10 in clinical tissue samples of ccRCC through tissue microarray immunohistochemical staining. The staining results indicated that the higher the clinical grade, the greater the staining intensity and positive area ratio of AKR1B10 in ccRCC (Fig. 2H-J). This result suggested that in the ccRCC tissue, the expression of AKR1B10 was upregulated as the clinical grade rises.

3.3 Knockdown of AKR1B10 suppresses the migration and invasion abilities of ccRCC cells in vitro and in vivo.

To investigate the effect of AKR1B10 on the phenotype of ccRCC cells, we knocked down the expression of AKR1B10 in 786-O-AR and 769-P-AR cells, and verified the knockdown efficiency at the mRNA and protein levels respectively through RT-qPCR (Fig. 3A) and Western Blot (Fig. 3B and Figure S1A). In addition, the Western blot results indicated that after knockdown of AKR1B10, the expressions of EMT-related proteins and anti-apoptotic proteins were downregulated, whereas the expression of pro-apoptotic proteins was upregulated (Fig. 3B and Figure S1A). To further clarify the biological function of AKR1B10 in ccRCC, we investigated the effects of AKR1B10 knockdown on the apoptosis, migration and invasion abilities of ccRCC cells. The wound healing assay (Fig. 3C and Figure S2A) and the transwell cell migration/invasion assay (Fig. 3D and Figure S2B) demenstrated that knockdown of AKR1B10 significantly inhibited the migration and invasion abilities of 786-O-AR and 769-P-AR cells. Meanwhile, the flow cytometry results indicated that after knocking down AKR1B10, the apoptosis rates of 786-O-AR and 769-P-AR cells increased significantly (Fig. 3E, F). Subsequently, we established a nude mouse tail vein lung metastasis model to further investigate the effect of AKR1B10 on the in vivo metastasis of ccRCC. The live imaging system detection showed that, compared with the control group, the fluorescence intensity in vivo (Fig. 3G, 3H) and lung tissues(Fig. 3I, 3J) of the AKR1B10 knockdown group was significantly reduced. Moreover, we performed hematoxylin and eosin (HE) staining on the isolated lung tissue and found that the cancer cells in the control group were arranged in a nest-like pattern closely together, with round nuclei deeply stained, and the lung alveolar structure was severely damaged (Fig. 3K). However, the AKR1B10 knockdown group had a reduced number of cancer cells, with a sparse distribution, and the lung alveolar structure was relatively intact (Fig. 3K). These above findings indicated that knockdown of AKR1B10 significantly inhibited the anti-apoptotic, migratory, and invasive capabilities of ccRCC cells in vitro, as well as metastatic ability in vivo.

3.4 Overexpression of AKR1B10 enhances the migration and invasion abilities of ccRCC cells.

To further elucidate the mechanistic role of AKR1B10, we transfected 786-O-P and 769-P-P cells with AKR1B10 overexpression plasmids. The overexpression efficiency was subsequently confirmed at both the protein and mRNA levels using Western blot (Fig. 4A and Fig. 4B) and RT-qPCR (Fig. 4C) respectively. The results showed that compared with the control group, the expression of AKR1B10 significantly

increased after transfection, indicating that the overexpressed plasmid was successfully transfected. In addition, the Western blot results demonstrated that after overexpression of AKR1B10, the expressions of EMT-related proteins and anti-apoptotic proteins were upregulated, whereas the expression of pro-apoptotic proteins was downregulated (Fig. 4A, B). Subsequently, the wound healing assay (Fig. 4D, E) and the transwell cell migration/invasion assay (Fig. 4F, G) indicated that overexpression of AKR1B10 significantly enhanced the migration and invasion abilities of 786-O-P and 769-P-P cells. Meanwhile, the flow cytometry results revealed that after overexpressing AKR1B10, the apoptosis rates of 786-O-P and 769-P-P cells decreased significantly (Fig. 4H, I). These findings suggested that overexpression of AKR1B10 had an opposite effect on the phenotype of ccRCC compared to knockdown of AKR1B10, further confirming the role of AKR1B10 in ccRCC.

3.5 TFAP2A, potentially upstream of AKR1B10, is overexpressed in metastasis ccRCC and correlates with poor prognosis.

To explore the upstream regulatory mechanism of AKR1B10 in anoikis-resistant ccRCC, we employed the UCSC database to predict its potential upstream transcription factors. Subsequently, we selected several candidate transcription factors by analyzing their binding scores in the JASPAR ChIP-seq dataset and their correlation with AKR1B10 expression levels in the TCGA-KIRC database (Supplementary Table 5). Ultimately, TFAP2A was predicted to be an upstream regulatory transcription factor of AKR1B10. The TCGA-KIRC database demonstrated that the expression of TFAP2A in tumor tissues of patients with T3/T4 stage ccRCC was significantly higher than that in patients with T1 stage (Fig. 5A). In addition, patients with lymph node metastasis (N1) and distant metastasis (M1) also exhibited higher expression levels (Fig. 5A). Moreover, patients with high expression of TFAP2A in ccRCC had poorer OS, DSS, and PFI (Fig. 5B). These findings suggested that highly expressed TFAP2A was closely associated with the metastatic potential and poor prognosis of ccRCC. Additionally, the Spearman correlation analysis revealed that the expression of TFAP2A and AKR1B10 in ccRCC was positively correlated (Fig. 5C). To verify the prediction and analysis results of bioinformatics, we measured the expression level of TFAP2A in the 786-O-AR, 769-P-AR and their parental cells. Western blot and RT-qPCR respectively indicated that, compared with the parental cells, the protein(Fig. 5D, E) and mRNA (Fig. 5F) levels of TFAP2A were elevated in the anoikis-resistant cells.

3.6 TFAP2A positively regulates the expression of AKR1B10 and regulates the downstream biological behaviors.

To verify that TFAP2A acts as an upstream transcription factor to regulate the expression of AKR1B10, we knocked down TFAP2A in 786-O-AR and 769-P-AR cells. Western blot and RT-qPCR results indicate that TFAP2A was successfully knocked down in 786-O-AR and 769-P-AR cells, and the mRNA and protein

levels of AKR1B10 subsequently decreased (Fig. 6A-C). To investigate the effect of TFAP2A on the phenotype of ccRCC, we conducted wound healing assay (Fig. 6D, E) and transwell cell migration/invasion assay (Fig. 6F, G). The results revealed that after knockdown of TFAP2A, the migration and invasion abilities of the anoikis-resistant cells were significantly suppressed. Additionally, according to the results of flow cytometry, knockdown of TFAP2A significantly inhibited the anti-apoptotic ability of anoikis-resistant cells(Fig. 6H, I).

On the other hand, overexpression of TFAP2A in 786-O-P and 769-P-P cells resulted in the upregulation of AKR1B10 expression at both the mRNA and protein levels (Fig. 7A-C). In addition, flow cytometry analysis revealed that after overexpression of TFAP2A, the anti-apoptotic ability of 786-O and 769-P cells was enhanced (Fig. 7D, E). Subsequently, according to wound healing assay (Fig. 7F, G) and transwell cell migration/invasion assay (Fig. 7H, 7I), the 786-O and 769-P cells exhibited enhanced migration and invasion capabilities compared with the control group.

Analyzing the effects of knockdown or overexpression of TFAP2A on the biological functions of ccRCC cells, we concluded that TFAP2A positively regulated AKR1B10 expression and promoted the malignant cell phenotype of ccRCC.

3.7 TFAP2A exerts its oncogenic function by binding to the promoter region of AKR1B10.

To verify that AKR1B10 mediates the effect of TFAP2A on the malignant phenotype of ccRCC cells, we conducted a rescue experiment in 786-O-AR and 769-P-AR cells, including control groups (shNC + Vector), TFAP2A knockdown group (shTFAP2A + Vector), and co-transfection group (shTFAP2A + AKR1B10-OE). Western blotting and RT-qPCR were performed to confirm the transfection efficiency (Fig. 8A, B and Figure S1B). In addition, Co-transfection with AKR1B10-OE partially restored the decreased expression levels of EMT-related and apoptosis-related proteins induced by TFAP2A knockdown (Fig. 8A and Figure S1B). The results of flow cytometry revealed that compared with the control group, the proportion of cell apoptosis significantly increased after knockdown of TFAP2A, while co-transfection with the overexpressed AKR1B10 plasmid partially reversed the suppressed anti-apoptotic ability (Fig. 8C, D). Subsequently, according to wound healing assay (Fig. 8E and Figure S2C) and transwell cell migration/invasion assay (Fig. 8F and Figure S2D), overexpression of AKR1B10 attenuated the inhibitory effect of TFAP2A knockdown on migration and invasion capabilities. These findings suggested that TFAP2A promotes the malignant cell phenotype of ccRCC by regulating AKR1B10. To further elucidate the mechanism underlying the positive regulation of AKR1B10 by TFAP2A, we identified three putative TFAP2A binding sites in the promoter region of AKR1B10 using the JASPAR database (Fig. 8H). Based on the sequences of the three potential binding sites, we constructed wild-type (WT) and mutant AKR1B10 promoter reporter gene plasmids (MUT1, MUT2, MUT3) and subsequently perform dual luciferase reporter assays (Fig. 8H, I). The result showed that compared with the control group, overexpression of TFAP2A significantly enhanced the luciferase activity in the WT, MUT1, and MUT3 transfection groups, whereas no significant change was observed in the MUT2

transfection group. Additionally, we further designed specific primers targeting the Target 2 fragment of the AKR1B10 promoter and employed the chromatin immunoprecipitation combined with quantitative PCR (ChIP-qPCR) (Fig. 8G). The qPCR results demonstrated that TFAP2A knockdown significantly reduced the enrichment of the AKR1B10 promoter region compared with the control group. In conclusion, these findings supported that TFAP2A directly bind to the promoter region of AKR1B10 and positively regulated its transcription.

4. Discussion

Clear cell renal cell carcinoma is the most common histopathological subtype of renal cell carcinoma, accounting for approximately 80% of all cases[31]. This subtype is characterized by a highly heterogeneous and invasive phenotype, an insidious onset[7], and a propensity for metastasis in up to one-third of cases[32]. Metastasis is the primary cause of mortality in ccRCC, and patients with metastases at different anatomical sites exhibit heterogeneous treatment responses and clinical outcomes[33]. Although the treatment landscape for metastatic RCC has undergone substantial transformation over the past decade, the current first-line treatment options predominantly comprise anti-PD-1 therapy plus anti-CTLA-4 therapy or tyrosine kinase inhibitor regimens[16]. However, the risk of tumor progression persists in patients with metastatic RCC during systemic therapy[34,35]. Thus, a comprehensive elucidation of the molecular mechanisms governing tumor metastasis represents a critical step toward breaking through the current clinical impasse.

Anoikis plays a critical role in tumor metastasis. Acquisition of anoikis resistance enhances the invasive capacity of tumor cells and promotes their survival within the circulatory system[18,36]. Accordingly, the present study is designed to investigate the role and underlying molecular mechanisms of anoikis resistance in metastatic ccRCC. Anoikis-resistant models were successfully established using the ccRCC cell lines 786-O and 769-P, which served as the platform for subsequent experiments. Notably, compared with their parental counterparts, anoikis-resistant cells exhibited markedly elevated expression of EMT associated proteins, suggesting that the EMT program was activated in anoikis-resistant ccRCC. EMT is a critical step in the metastasis of malignant tumor cells, and blockade of this process has been shown to suppress tumor cell invasion and metastatic potential[37–39]. Thus, our findings established a mechanistic link between anoikis resistance and metastatic progression in ccRCC, suggesting that the acquisition of anoikis resistance phenotype drives tumor metastasis.

To screen for differentially expressed genes and potential signaling pathways between ccRCC parental cells and anoikis-resistant counterparts, mRNA transcriptome sequencing was performed on 786-O-P and 786-O-AR cells. Integrated analysis with the TCGA-KIRC dataset reveals that AKR1B10 was highly expressed in AR cells, and its expression levels in ccRCC patients increased progressively with clinical stage. Specifically, AKR1B10 expression was significantly higher in tumor tissues from patients at T3/T4 stages than in those at T1/T2 stages, and similarly elevated levels were observed in patients with lymph node or distant metastasis. These results suggested that AKR1B10 upregulation is closely associated

with the metastatic potential of ccRCC. Furthermore, patients with higher AKR1B10 expression exhibited poorer prognosis. Collectively, these findings indicated that AKR1B10 may serve as a critical regulator of anoikis resistance and metastasis in ccRCC.

AKR1B10 is a NADPH-dependent reductase belonging to the aldo-keto reductase family 1, also known as aldose reductase-like protein-1[40]. AKR1B10 catalyzes the reduction of aldehydes and ketones, thereby mitigating protein and DNA damage[41]. In addition, it influences lipid metabolism by inhibiting acetyl-CoA and participates in the regulation of various cellular physiological activities[42,43]. Accumulating evidence has demonstrated that AKR1B10 is upregulated in a variety of malignancies, including hepatocellular carcinoma, breast cancer, and lung cancer, and that its overexpression is closely associated with tumor progression and metastasis[41,44–46]. In RCC, AKR1B10 may serve as a bridge linking tumor metabolism and tumor immunity, and has been applied in the construction of prognostic prediction models[47]. Meanwhile, it is highly expressed in fumarate hydratase (FH)-deficient hereditary RCC and is recognized as a highly sensitive and specific diagnostic biomarker[48,49]. In addition, recent studies have reported that AKR1B10, potentially regulated by DDX24, may mediate the progression of clear cell RCC through the EMT pathway[50]. However, the precise mechanisms underlying the role of AKR1B10 in anoikis resistance in ccRCC remain to be further elucidated.

786-O-AR,769-P-AR and their parental cell lines (786-O and 769-P) were employed in this study. RT-qPCR and Western blot analyses reveal that AKR1B10 expression was significantly elevated in AR cells compared with their parental counterparts. To validate this finding at the tissue level, tissue microarrays derived from ccRCC patients of different pathological grades were analyzed by immunohistochemistry, which demonstrated that higher AKR1B10 staining scores were associated with higher tumor grades. Subsequently, to explore the upstream regulatory mechanisms of AKR1B10, the UCSC Genome Browser (https://genome.ucsc.edu/) and JASPAR (https://jaspar.elixir.no/) databases were utilized to predict candidate transcription factors governing AKR1B10 expression. Based on a combination of binding site scores, Spearman correlation coefficients, and significance P-values, TFAP2A was ultimately selected for further investigation.

TFAP2A is a member of the activator protein 2 (AP-2) family of transcription factors. Its encoded protein specifically recognizes and binds to the consensus sequence 5'-GCCNNNGGC-3' in promoter regions, and plays a critical role in the regulation of embryonic development and tumorigenesis[51,52]. Notably, TFAP2A has been demonstrated to play a key role in the regulation of the EMT signaling pathway in tumors[51,53]. Previous studies have demonstrated that TFAP2A plays a critical role in the progression and drug resistance of multiple malignancies, including breast cancer, non-small cell lung cancer, and colorectal cancer[54–56]. In ccRCC, TFAP2A has also been shown to promote ccRCC progression by regulating lipid metabolism[57]. Meanwhile, TFAP2A has been reported to cooperate with EP300 as a co-transcription factor to promote PD-L1 transcription in ccRCC[58]. Nevertheless, the precise molecular mechanisms underlying the role of TFAP2A in ccRCC remain to be fully clarified.

In this study, bioinformatics analysis revealed that TFAP2A expression in ccRCC increased progressively with clinical stage, and that high TFAP2A expression was significantly correlated with poor patient prognosis. At the cellular level, TFAP2A was markedly upregulated in anoikis-resistant ccRCC cells compared with their parental counterparts. Knockdown of TFAP2A in 786-O-AR and 769-P-AR cells resulted in reduced AKR1B10 expression, increased apoptosis, and impaired migration and invasion capabilities. Conversely, further overexpression of AKR1B10 partially reversed these phenotypic changes, suggesting that TFAP2A exerted its biological effects at least in part through the regulation of AKR1B10. Subsequently, dual-luciferase reporter assays and chromatin immunoprecipitation (ChIP) assays were performed to elucidate the molecular interaction between TFAP2A and AKR1B10. The results demonstrated that TFAP2A directly binds to the promoter region of AKR1B10 and positively regulated its transcription, thereby inducing EMT and driving anoikis resistance and metastatic progression in ccRCC.

Finally, several limitations of this study should be acknowledged. Although the transcriptional regulatory relationship between TFAP2A and AKR1B10 is confirmed, the upstream signaling pathways that govern the activity or expression of TFAP2A have not yet been elucidated. The transcriptional activity of TFAP2A may be influenced by phosphorylation, protein stability regulation, or other co-activators[59], and the precise roles of these factors in ccRCC warrant further investigation. In addition, reverse pharmacological validation using AKR1B10-specific small-molecule inhibitors is not performed in this study. The use of classical non-selective synthetic inhibitors of AKR1B10, such as sorbinil[60], in future studies would provide more direct pharmacological evidence for AKR1B10-targeted intervention strategies.

Nevertheless, the present study is the first to report the regulatory role of the TFAP2A/AKR1B10 axis in anoikis resistance and metastasis in ccRCC, and to elucidate the novel mechanism by which TFAP2A promotes ccRCC metastasis through transcriptional activation of AKR1B10 at the molecular level. However, the translation of these fundamental findings into clinical applications necessitates substantial further investigation. Future studies are warranted to deepen the mechanistic understanding and optimize animal models, with the aim of providing a more robust theoretical basis for the diagnosis and treatment of ccRCC metastasis.

Conclusion

Anoikis resistance enhanced the migration and invasion capabilities of ccRCC cells in vitro. AKR1B10 and its upstream transcription factor TFAP2A were highly expressed in metastatic ccRCC and are significantly correlated with poor patient prognosis. TFAP2A bind to the promoter region of AKR1B10 and positively activated its transcription, thereby inducing EMT and driving anoikis resistance and metastatic progression in ccRCC. Collectively, these findings suggested that AKR1B10 may serve as a promising target for the diagnosis, monitoring, and treatment of metastatic ccRCC.

Abbreviations

Abbreviation	Full form
RCC	Renal cell carcinoma
ccRCC	Clear cell renal cell carcinoma
AKR1B10	Aldo-keto reductase family 1 member B10
TFAP2A	Transcription factor activator protein-2 alpha
mRNA	messenger RNA
siRNA	small interfering RNA
shRNA	short hairpin RNA
EMT	Epithelial-mesenchymal transition
AR	Anoikis resistant
NC	Negative control
PCR	Polymerase chain reaction
RT-qPCR	Real-time quantitative PCR
cDNA	complementary DNA
PBS	Phosphate-buffered saline
FBS	Fetal bovine serum
BCA	Bicinchoninic acid
TCGA	The cancer genome atlas
N-Cad	N-cadherin
SLUG	Zinc finger protein SNAI2
MMP-2	Matrix metalloproteinase-2
Mcl-1	Myeloid cell leukemia 1
Bcl-2	B-cell lymphoma 2
OS	Overall survival
DSS	Disease-specific survival
PFI	Progression-free interval
ICIs	Immune checkpoint inhibitors
TKIs	Tyrosine kinase inhibitors
ECM	Extracellular matrix

WT	Wild type
KIRC	Kidney renal clear cell carcinoma
PD-1	Programmed cell death protein 1
CTLA-4	Cytotoxic T-lymphocyte-associated protein 4
HE	Hematoxylin and eosin
IRS	Immunoreactive score
ChIP	Chromatin immunoprecipitation

Declarations

Ethics approval and consent to participate

The operation of animals in our study were approved by the Medical Ethics Committee of the First Affiliated Hospital, Zhejiang University School of Medicine.

Consent for publication

Consent for publication was obtained from the participants.

Availability of data and materials

The data that support the findings of this study are available in the supplementary material of this article.

Competing interests

The authors declare that they have no competing interests.

Funding

This work was supported by grants from the National Natural Science Foundation of China (82273132, 82573582), Key Research and Development Program of Zhejiang Province (2025C02071).

Authors' contributions

The conception and design of the study: Ben Liu; The acquisition of data: Jihuan Yuan, Yuxiao Li, Fenghao Zhang, Xinyang Niu; Analysis and interpretation of data: Jiazhu Sun, Yuchen Shi, Suyuelin Huang, Kai Yu, Jiawei Zhang, Xueyou Ma; Drafting the article or revising it critically for important intellectual content: Jihuan Yuan, Yuxiao Li, Dingheng Lu; Final approval of the version to be submitted: all authors.

Acknowledgements

We are grateful for the supports from Jie Fang in all animal experiments.

Supporting Information

Supporting Information is available from the corresponding author.

Declaration of Generative AI and AI-assisted technologies in the writing process

During the preparation of the manuscript, we utilized “DeepSeek” AI to enhance the linguistic logic and coherence of the text. Following the use of this tool, we carefully revised and modified the content as necessary, and we assume full responsibility for all content in this publication.

Clinical trial number

Not applicable

References

1. Bex A, Ghanem YA, Albiges L et al (2025) European Association of Urology Guidelines on Renal Cell Carcinoma: The 2025 Update. Eur Urol 87(6):683–696. 10.1016/j.eururo.2025.02.020
2. Ferlay J, Colombet M, Soerjomataram I et al (2018) Cancer incidence and mortality patterns in Europe: Estimates for 40 countries and 25 major cancers in 2018. Eur J Cancer 103:356–387. 10.1016/j.ejca.2018.07.005
3. Sung H, Filho AM, Laversanne M et al (2026) Global cancer statistics 2024: GLOBOCAN estimates of incidence and mortality worldwide for 34 cancers in 186 countries. CA Cancer J Clin 76(4):e70090. 10.3322/caac.70090
4. Cirillo L, Innocenti S, Becherucci F (2024) Global epidemiology of kidney cancer. Nephrol Dial Transpl 39(6):920–928. 10.1093/ndt/gfae036
5. Wu Y, He S, Cao M et al (2024) Comparative analysis of cancer statistics in China and the United States in 2024. Chin Med J (Engl) 137(24):3093–3100. 10.1097/CM9.0000000000003442
6. Bukavina L, Bensalah K, Bray F et al (2022) Epidemiology of Renal Cell Carcinoma: 2022 Update. Eur Urol 82(5):529–542. 10.1016/j.eururo.2022.08.019
7. Huang B, Ren J, Ma Q et al (2024) A novel peptide PDHK1-241aa encoded by circPDHK1 promotes ccRCC progression via interacting with PPP1CA to inhibit AKT dephosphorylation and activate the AKT-mTOR signaling pathway. Mol Cancer 23(1):34. 10.1186/s12943-024-01940-0
8. Zhang X, Zhang G, Xu L, Prediction of World Health Organization /International Society of Urological Pathology (WHO/ISUP) et al (2023) Pathological Grading of Clear Cell Renal Cell Carcinoma by Dual-Layer Spectral CT. Acad Radiol 30(10):2321–2328. 10.1016/j.acra.2022.12.002
9. Choueiri TK, Motzer RJ (2017) Systemic Therapy for Metastatic Renal-Cell Carcinoma. N Engl J Med 376(4):354–366. 10.1056/NEJMra1601333

10. Rathmell WK, Rumble RB, Van Veldhuizen PJ et al (2022) Management of Metastatic Clear Cell Renal Cell Carcinoma: ASCO Guideline. J Clin Oncol 40(25):2957–2995. 10.1200/JCO.22.00868
11. Powles T, Albiges L, Bex A et al (2024) Renal cell carcinoma: ESMO Clinical Practice Guideline for diagnosis, treatment and follow-up. Ann Oncol 35(8):692–706. 10.1016/j.annonc.2024.05.537
12. Atkins MB, Clark JI, Quinn DI (2017) Immune checkpoint inhibitors in advanced renal cell carcinoma: experience to date and future directions. Ann Oncol 28(7):1484–1494. 10.1093/annonc/mdx151
13. Jin J, Xie Y, Zhang JS et al (2023) Sunitinib resistance in renal cell carcinoma: From molecular mechanisms to predictive biomarkers. Drug Resist Updat 67:100929. 10.1016/j.drup.2023.100929
14. Rosellini M, Marchetti A, Mollica V, Rizzo A, Santoni M, Massari F (2023) Prognostic and predictive biomarkers for immunotherapy in advanced renal cell carcinoma. Nat Rev Urol 20(3):133–157. 10.1038/s41585-022-00676-0
15. Sharma R, Kadife E, Myers M, Kannourakis G, Prithviraj P, Ahmed N (2021) Determinants of resistance to VEGF-TKI and immune checkpoint inhibitors in metastatic renal cell carcinoma. J Exp Clin Cancer Res 40(1):186. 10.1186/s13046-021-01961-3
16. Barragan-Carrillo R, Saad E, Saliby RM et al (2025) First and Second-line Treatments in Metastatic Renal Cell Carcinoma. Eur Urol 87(2):143–154. 10.1016/j.eururo.2024.10.019
17. Chiarugi P, Giannoni E (2008) Anoikis: a necessary death program for anchorage-dependent cells. Biochem Pharmacol 76(11):1352–1364. 10.1016/j.bcp.2008.07.023
18. Shaw P, Dey Bhowmik A, Gopinatha Pillai MS, Robbins N, Dwivedi SKD, Rao G (2025) Anoikis resistance in Cancer: Mechanisms, therapeutic strategies, potential targets, and models for enhanced understanding. Cancer Lett 624:217750. 10.1016/j.canlet.2025.217750
19. Wang Y, Cheng S, Fleishman JS et al (2024) Targeting anoikis resistance as a strategy for cancer therapy. Drug Resist Updat 75:101099. 10.1016/j.drup.2024.101099
20. Kim YN, Koo KH, Sung JY, Yun UJ, Kim H (2012) Anoikis Resistance: An Essential Prerequisite for Tumor Metastasis. Int J Cell Biol 2012:306879. 10.1155/2012/306879
21. Wang Y, Cheng S, Fleishman JS et al (2024) Targeting anoikis resistance as a strategy for cancer therapy. Drug Resist Updat 75:101099. 10.1016/j.drup.2024.101099
22. Khan SU, Fatima K, Malik F (2022) Understanding the cell survival mechanism of anoikis-resistant cancer cells during different steps of metastasis. Clin Exp Metastasis 39(5):715–726. 10.1007/s10585-022-10172-9
23. Simpson CD, Anyiwe K, Schimmer AD (2008) Anoikis resistance and tumor metastasis. Cancer Lett 272(2):177–185. 10.1016/j.canlet.2008.05.029
24. Yu Y, Liu B, Li X et al (2022) ATF4/CEMIP/PKCα promotes anoikis resistance by enhancing protective autophagy in prostate cancer cells. Cell Death Dis 13(1):46. 10.1038/s41419-021-04494-x
25. Song J, Liu Y, Liu F et al (2021) The 14-3-3σ protein promotes HCC anoikis resistance by inhibiting EGFR degradation and thereby activating the EGFR-dependent ERK1/2 signaling pathway. Theranostics 11(3):996–1015. 10.7150/thno.51646

26. Jin L, Chun J, Pan C et al (2018) The PLAG1-GDH1 Axis Promotes Anoikis Resistance and Tumor Metastasis through CamKK2-AMPK Signaling in LKB1-Deficient Lung Cancer. Mol Cell 69(1):87–99e7. 10.1016/j.molcel.2017.11.025
27. Dai Y, Zhang X, Ou Y et al (2023) Anoikis resistance–protagonists of breast cancer cells survive and metastasize after ECM detachment. Cell Commun Signal 21(1):190. 10.1186/s12964-023-01183-4
28. Zhang P, Xing Z, Li X et al (2016) Tyrosine receptor kinase B silencing inhibits anoikis–resistance and improves anticancer efficiency of sorafenib in human renal cancer cells. Int J Oncol 48(4):1417–1425. 10.3892/ijo.2016.3356
29. Sakamoto S, Schwarze S, Kyprianou N (2011) Anoikis disruption of focal adhesion-Akt signaling impairs renal cell carcinoma. Eur Urol 59(5):734–744. 10.1016/j.eururo.2010.12.038
30. Niu X, Lu D, Zhan W et al (2025) miR-9-5p/HMMR regulates the tumorigenesis and progression of clear cell renal cell carcinoma through EMT and JAK1/STAT1 signaling pathway. J Transl Med 23(1):36. 10.1186/s12967-024-05988-w
31. Young M, Jackson-Spence F, Beltran L et al (2024) Renal cell carcinoma. Lancet 404(10451):476–491. 10.1016/S0140-6736(24)00917-6
32. Jonasch E, Walker CL, Rathmell WK (2021) Clear cell renal cell carcinoma ontogeny and mechanisms of lethality. Nat Rev Nephrol 17(4):245–261. 10.1038/s41581-020-00359-2
33. Zhou X, Li R, Lai M, Lai C (2025) Exploring molecular and cellular mechanisms of Pre-Metastatic niche in renal cell carcinoma. Mol Cancer 24:121. 10.1186/s12943-025-02315-9
34. Yoshida K, Kondo T, Iizuka J et al (2026) Clinical evaluation of medical and surgical complete responses in metastatic renal cell carcinoma treated with immune checkpoint inhibitor combination therapy. Int J Clin Oncol 31(4):683–694. 10.1007/s10147-026-02981-9
35. Gulati S, Nardo L, Lara PN (2025) Strategies for Treatment De-escalation in Metastatic Renal Cell Carcinoma. Eur Urol Focus 11(3):411–416. 10.1016/j.euf.2025.05.014
36. Liu M, Yang J, Xu B, Zhang X (2021) Tumor metastasis: Mechanistic insights and therapeutic interventions. *MedComm (2020)*. ;2(4):587–617. 10.1002/mco2.100
37. Greenburg G, Hay ED (1982) Epithelia suspended in collagen gels can lose polarity and express characteristics of migrating mesenchymal cells. J Cell Biol 95(1):333–339. 10.1083/jcb.95.1.333
38. Davis FM, Stewart TA, Thompson EW, Monteith GR (2014) Targeting EMT in cancer: opportunities for pharmacological intervention. Trends Pharmacol Sci 35(9):479–488. 10.1016/j.tips.2014.06.006
39. Bakir B, Chiarella AM, Pitarresi JR, Rustgi AK (2020) EMT, MET, Plasticity, and Tumor Metastasis. Trends Cell Biol 30(10):764–776. 10.1016/j.tcb.2020.07.003
40. Penning TM (2015) The aldo-keto reductases (AKRs): Overview. Chem Biol Interact 234:236–246. 10.1016/j.cbi.2014.09.024
41. Shen Y, Qiu A, Huang X et al (2024) AKR1B10 and digestive tumors development: a review. Front Immunol 15:1462174. 10.3389/fimmu.2024.1462174

42. van Weverwijk A, Koundouros N, Iravani M et al (2019) Metabolic adaptability in metastatic breast cancer by AKR1B10-dependent balancing of glycolysis and fatty acid oxidation. Nat Commun 10:2698. 10.1038/s41467-019-10592-4
43. Endo S, Matsunaga T, Nishinaka T (2021) The Role of AKR1B10 in Physiology and Pathophysiology. Metabolites 11(6):332. 10.3390/metabo11060332
44. Liu W, Song J, Du X et al (2019) AKR1B10 (Aldo-keto reductase family 1 B10) promotes brain metastasis of lung cancer cells in a multi-organ microfluidic chip model. Acta Biomater 91:195–208. 10.1016/j.actbio.2019.04.053
45. Qu J, Li J, Zhang Y et al (2021) AKR1B10 promotes breast cancer cell proliferation and migration via the PI3K/AKT/NF-κB signaling pathway. Cell Biosci 11:163. 10.1186/s13578-021-00677-3
46. Yu Y, Li Y, Zhou L, Cheng X, Gong Z (2024) Hepatic stellate cells promote hepatocellular carcinoma development by regulating histone lactylation: Novel insights from single-cell RNA sequencing and spatial transcriptomics analyses. Cancer Lett 604:217243. 10.1016/j.canlet.2024.217243
47. Li L, Chao Z, Waikeong U et al (2023) Metabolic classifications of renal cell carcinoma reveal intrinsic connections with clinical and immune characteristics. J Transl Med 21(1):146. 10.1186/s12967-023-03978-y
48. Ooi A, Wong JC, Petillo D et al (2011) An antioxidant response phenotype shared between hereditary and sporadic type 2 papillary renal cell carcinoma. Cancer Cell 20(4):511–523. 10.1016/j.ccr.2011.08.024
49. Zheng L, Zhang X, Pan X et al (2023) AKR1B10 Is a New Sensitive and Specific Marker for Fumarate Hydratase-Deficient Renal Cell Carcinoma. Mod Pathol 36(11):100303. 10.1016/j.modpat.2023.100303
50. Li Z, Li X, Yang M et al (2025) DDX24 inhibits clear cell renal cell carcinoma progression by directly regulating AKR1B10. Cell Signal 132:111804. 10.1016/j.cellsig.2025.111804
51. Jin C, Luo Y, Liang Z et al (2023) Crucial role of the transcription factors family activator protein 2 in cancer: current clue and views. J Transl Med 21:371. 10.1186/s12967-023-04189-1
52. Eckert D, Buhl S, Weber S, Jäger R, Schorle H (2005) The AP-2 family of transcription factors. Genome Biol 6(13):246. 10.1186/gb-2005-6-13-246
53. Dimitrova Y, Gruber AJ, Mittal N et al (2017) TFAP2A is a component of the ZEB1/2 network that regulates TGFB1-induced epithelial to mesenchymal transition. Biol Direct 12(1):8. 10.1186/s13062-017-0180-7
54. Zou H, Luo J, Guo Y et al (2024) Tyrosine phosphorylation-mediated YAP1-TFAP2A interactions coordinate transcription and trastuzumab resistance in HER2 + breast cancer. Drug Resist Updat 73:101051. 10.1016/j.drup.2024.101051
55. Wang DG, Gao J, Wang J et al (2024) TFAP2A drives non-small cell lung cancer (NSCLC) progression and resistance to targeted therapy by facilitating the ESR2-mediated MAPK pathway. Cell Death Discov 10(1):491. 10.1038/s41420-024-02251-5

56. Gao X, Huang Y, Wei T et al (2025) TFAP2A-regulated CRNDE enhances colon cancer progression and chemoresistance via RIPK3 interaction. Funct Integr Genomics 25(1):36. 10.1007/s10142-025-01545-w
57. Shi J, Miao D, Lv Q et al (2023) The m6A modification-mediated OGDHL exerts a tumor suppressor role in ccRCC by downregulating FASN to inhibit lipid synthesis and ERK signaling. Cell Death Dis 14(8):560. 10.1038/s41419-023-06090-7
58. Zhang W, Zhao E, Li Z et al (2024) Hexokinase HK3-mediated O-GlcNAcylation of EP300: a key regulator of PD-L1 expression and immune evasion in ccRCC. Cell Death Dis 15(8):613. 10.1038/s41419-024-06921-1
59. Kanoura A, Giakountis A, Filippopoulou C et al (2025) Interaction of TFAP2A with the Ku70/80 complex is crucial for HIF-dependent activation of hypoxia-inducible genes. FEBS J 292(16):4333–4352. 10.1111/febs.70025
60. Maccari R, Ottanà R (2025) In Search for Inhibitors of Human Aldo-Keto Reductase 1B10 (AKR1B10) as Novel Agents to Fight Cancer and Chemoresistance: Current State-of-the-Art and Prospects. J Med Chem 68(2):860–885. 10.1021/acs.jmedchem.4c01116

Figures

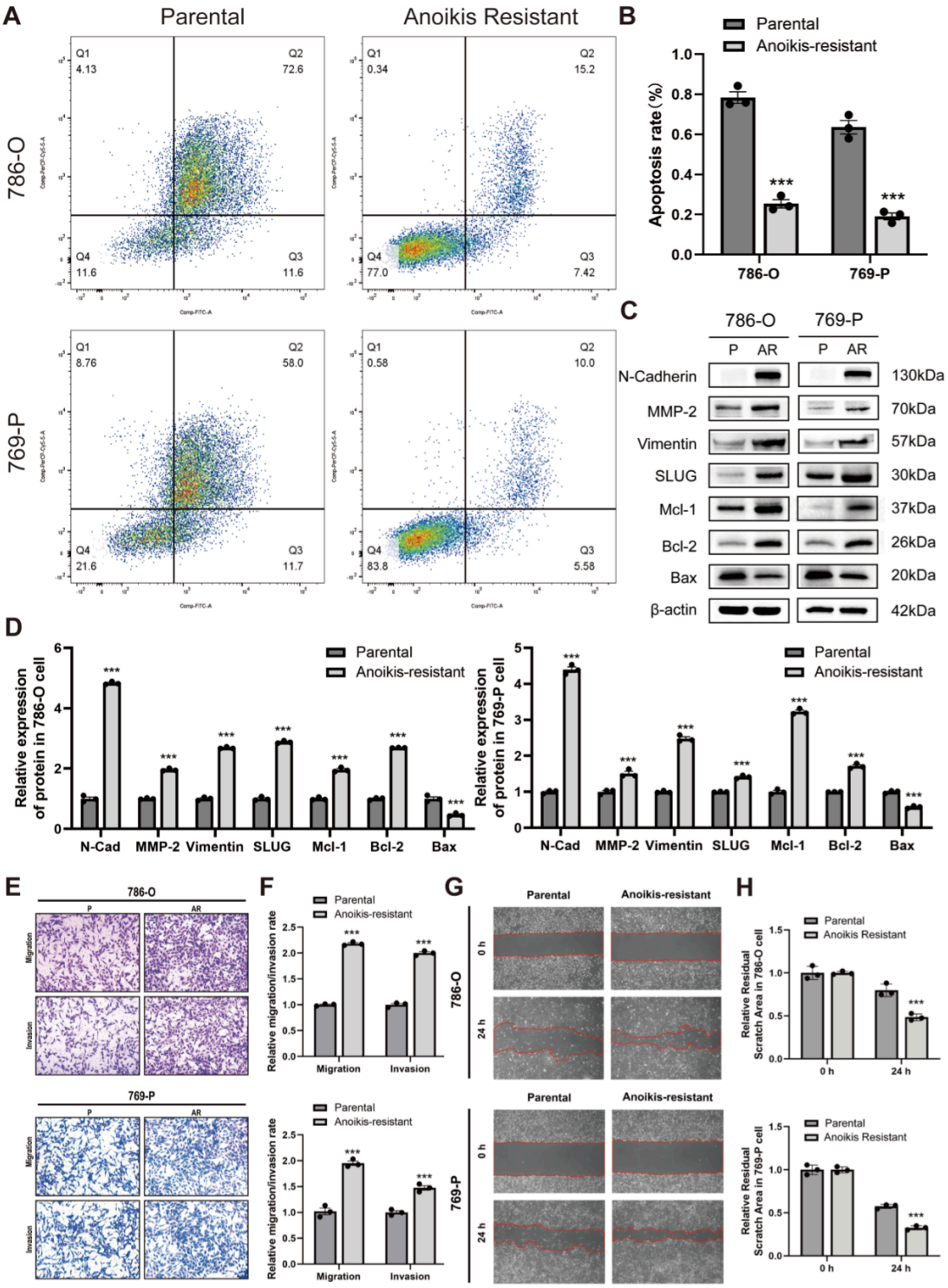


Figure 1

Establishment of an anoikis-resistant clear cell renal cell carcinoma model A, B FITC/PI double staining combined with flow cytometry demonstrated 786-O-AR and 769-P-AR cells possessed stronger anti-apoptotic capabilities. **C, D** Western blot analysis revealed that in 786-O-AR and 769-P-AR cells, the expressions of N-Cadherin, MMP-2, Vimentin, SLUG, Mcl-1 and Bcl-2 were upregulated, while the expression of Bax was downregulated. *** for $p < 0.001$. Data are represented as mean ± SD (n = 3 per

group). **E, F** The migration and invasion capacity of 786-O-AR and 769-P-AR cells were assessed using a transwell cell migration/invasion assay. **G, H** The migratory capacity of 786-O-AR and 769-P-AR cells was assessed using a wound healing assay.

All data in this figure are represented as mean +/- SD (n = 3 per group).

*** for p < 0.001. Statistical significance for B, D, F and H is determined using one-way ANOVA.

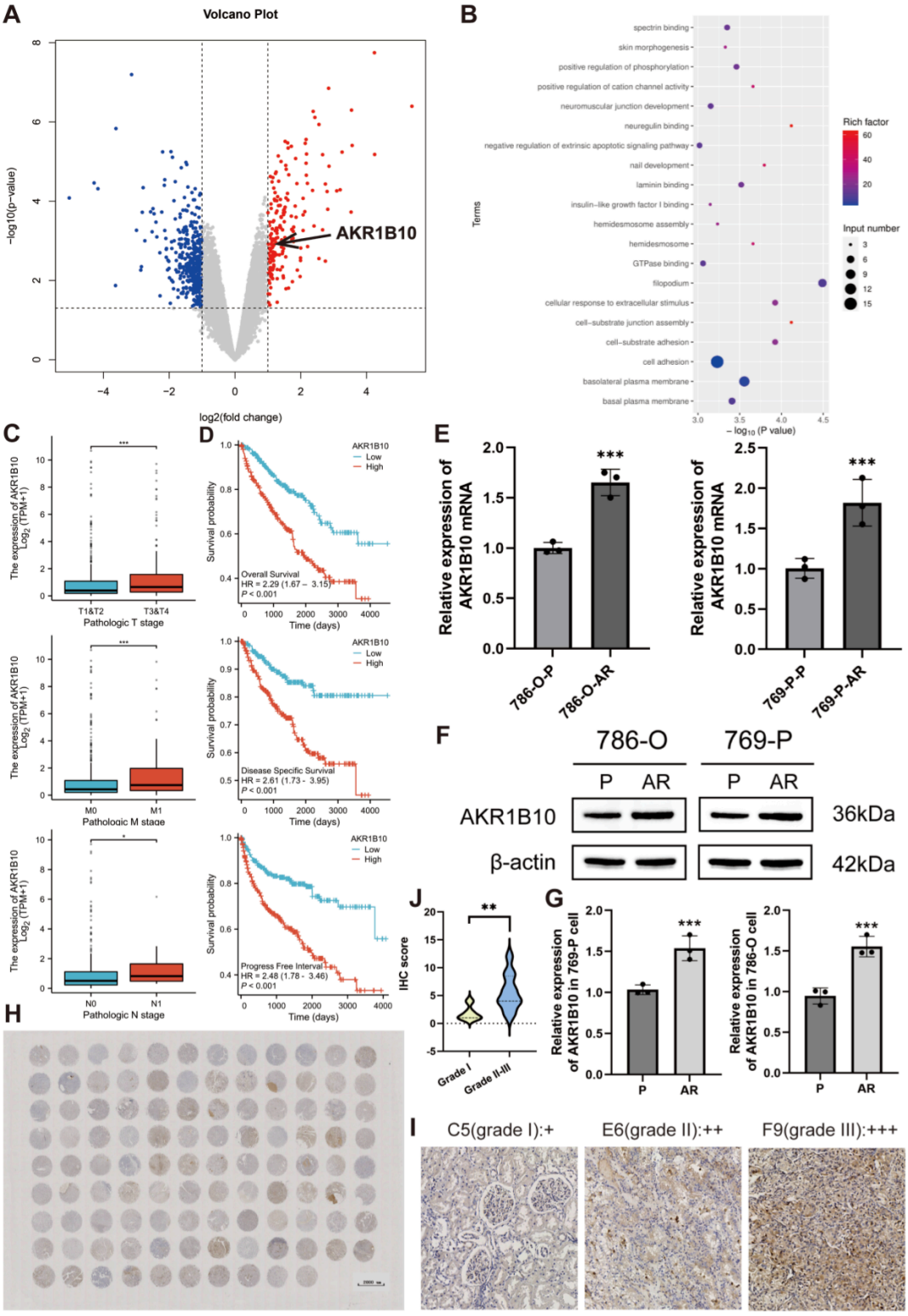


Figure 2

AKR1B10 is highly expressed in metastatic ccRCC and is associated with poor prognosis. A, B The RNA sequencing results of 786-O-P and 786-O-AR. A: Differentially expressed genes between 786-O and 786-O-AR. B: Results of GO enrichment analysis. **C** According to the statistics from the TCGA-KIRC database, the expression differences of AKR1B10 at different clinical stages of ccRCC. (*P < 0.05, ***P < 0.001). **D** OS, DSS, and PFI were analyzed according to high or low expression of AKR1B10. **E-G** The mRNA and protein expression of AKR1B10 were elevated in ccRCC. **H-J** The expression of AKR1B10 in clinical tissue microarrays of ccRCC. H: The results of immunohistochemical staining of the tissue microarrays. I: Representative immunohistochemical staining images. (magnification: ×200). J: The results of the comprehensive scoring based on the immunoreactive score (IRS) method for the staining intensity and the percentage of positive cells. (mean ± SD□**P < 0.01).

All data in this figure are represented as mean +/- SD (n = 3 per group).

*for p< 0.05, ** for p < 0.01, and *** for p < 0.001. Statistical significance for C is determined using the Wilcoxon rank-sum test. The log-rank test for D. One-way ANOVA for E, G and J.

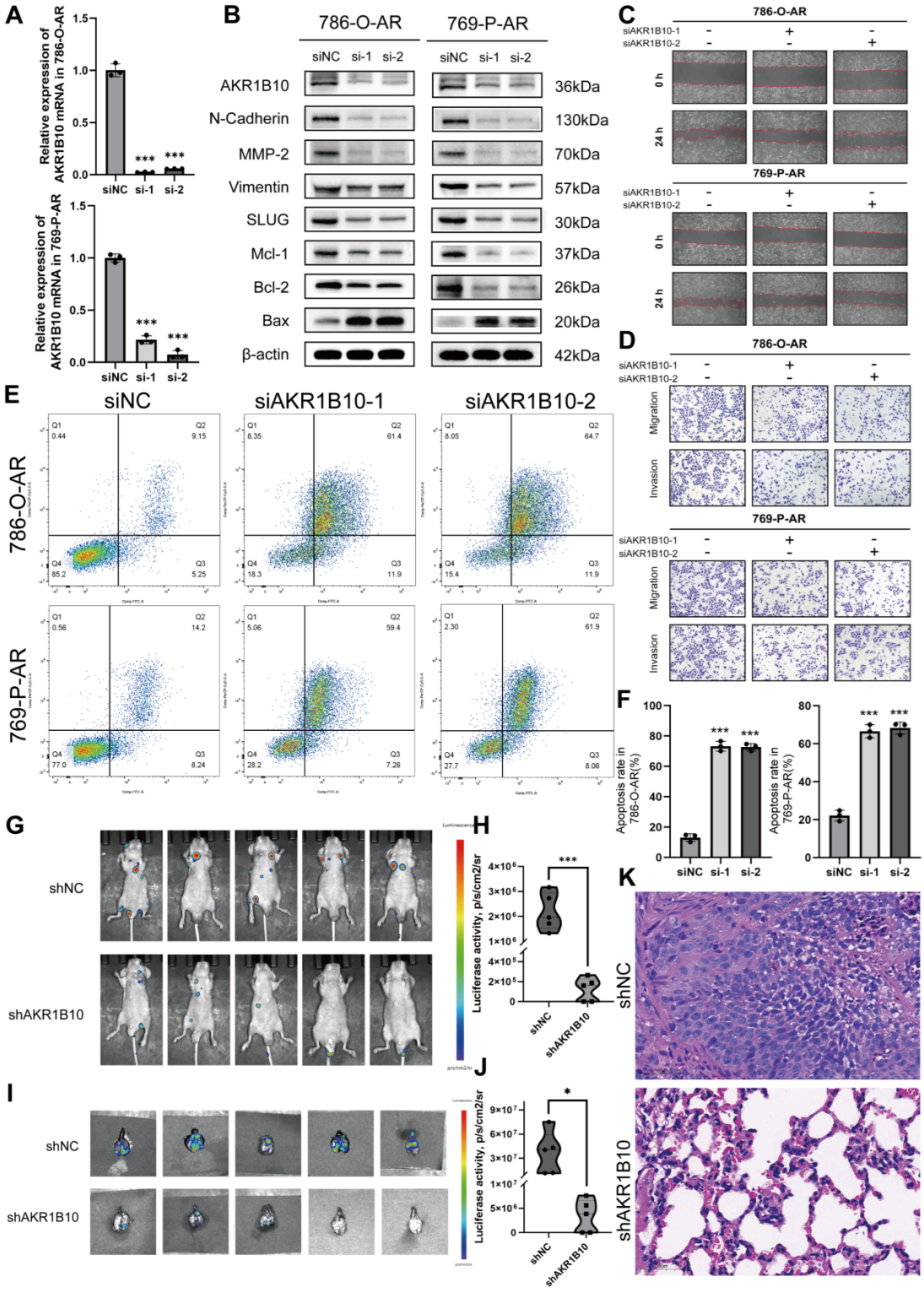


Figure 3

Knockdown of AKR1B10 suppresses the migration and invasion abilities of ccRCC cells in vitro and in vivo. A The RT-qPCR experiment demonstrated that after transfection with shAKR1B10 in 786-O-AR and 769-P-AR cells, AKR1B10 was knocked down at the transcriptional level. **B** The Western blot experiment showed the differential expression of EMT-related proteins and apoptosis-related proteins after shAKR1B10 transfection in 786-O-AR and 769-P-AR cells. **C** The migratory capacity was assessed using

a wound healing assay. **D** The migration and invasion capacity was assessed using a transwell cell migration/invasion assay. **E,F**FITC/PI double staining combined with flow cytometry demonstrated that after knockdown of AKR1B10, the anti-apoptotic capabilities of 786-O-AR and 769-P-AR cells were suppressed. **G, H** Representative images and fluorescence intensities from the tail vein injection transfer model of ccRCC in Balb/c nude mice. **I, J** Ex vivo imaging and fluorescence intensity of lung tissues from the tail vein injection transfer model of ccRCC in Balb/c nude mice. **K** Representative HE staining images of ex vivo lung tissues from the tail vein injection transfer model of ccRCC in Balb/c nude mice.

Data for A-F in this figure are represented as mean +/- SD (n = 3 per group). Mean +/- SD (n = 5 per group) for G-K.

* for $p < 0.05$, *** for $p < 0.001$. Statistical significance for A, F, H and J is determined using one-way ANOVA.

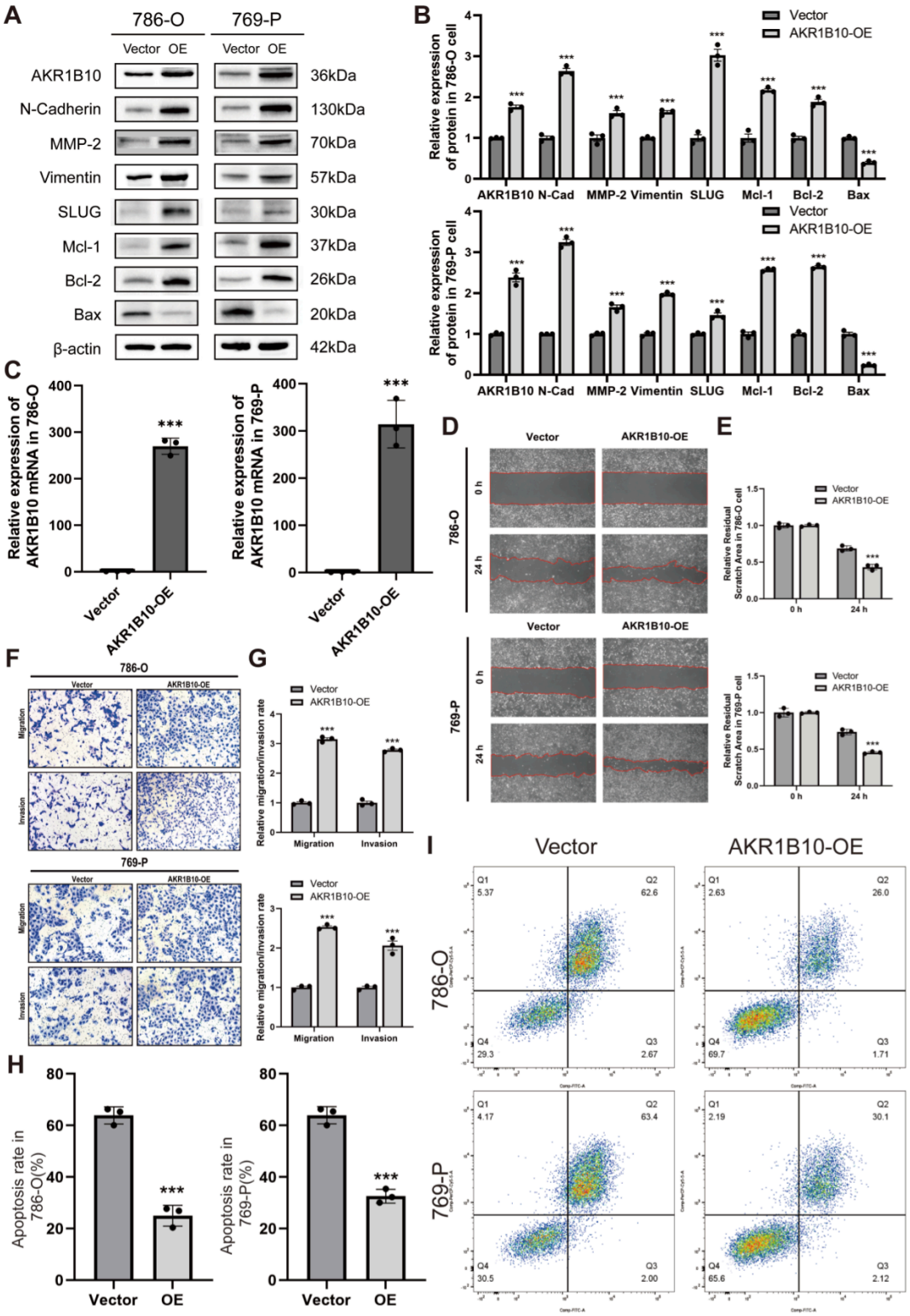


Figure 4

Overexpression of AKR1B10 enhances the migration and invasion abilities of ccRCC cells. A, B The Western blot experiment showed the differential expression of EMT-related proteins and apoptosis-related proteins after transfection with AKR1B10-OE plasmids in 786-O and 769-P cells. **C** The RT-qPCR experiment demonstrated that after transfection with AKR1B10-OE plasmids in 786-O and 769-P cells, AKR1B10 was overexpressed at the transcriptional level. **D, E** The migratory capacity of 786-O and 769-P

cells after overexpression of AKR1B10 was assessed using a wound healing assay. **F, G** The migration and invasion capacity of 786-O and 769-P cells after overexpression of AKR1B10 was assessed using a transwell cell migration/invasion assay. **H-I** FITC/PI double staining combined with flow cytometry demonstrated that after overexpression of AKR1B10, the anti-apoptotic capabilities of 786-O and 769-P cells were enhanced.

All data in this figure are represented as mean +/- SD (n = 3 per group).

*** for $p < 0.001$. Statistical significance for B, C, E, G and H is determined using one-way ANOVA.

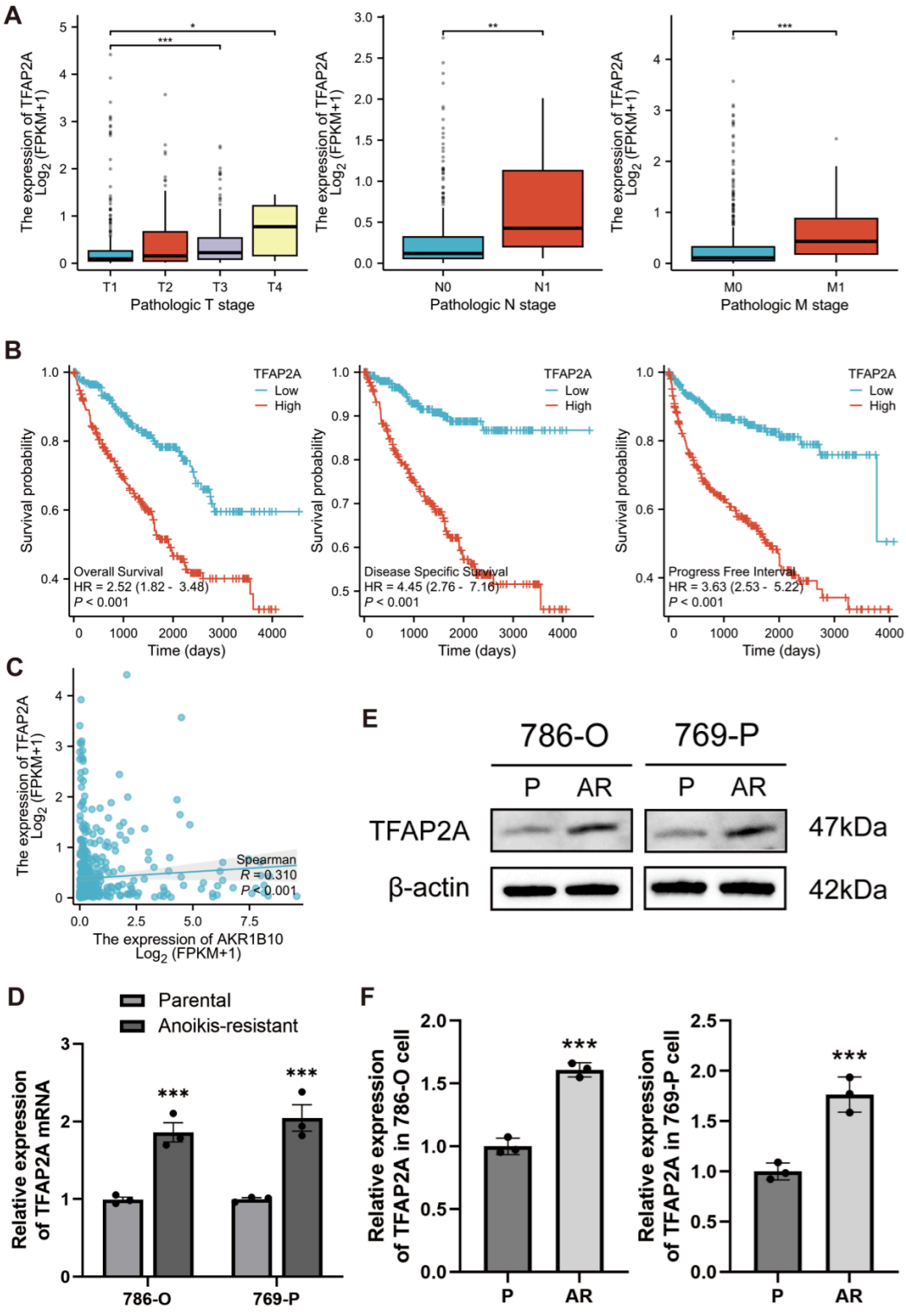


Figure 5

TFAP2A upregulation in metastasis ccRCC and its association with prognosis. A The expression differences of TFAP2A at different clinical stages of ccRCC. **B** OS, DSS, and PFI were analyzed according to high or low expression of TFAP2A. **C** Scatter plot of the clinical correlation between TFAP2A and AKR1B10. **D-F** The mRNA and protein expression of TFAP2A were elevated in 786-O-AR and 769-P-AR.

All data in this figure are represented as mean +/- SD (n = 3 per group).

*for p< 0.05, ** for p < 0.01, and *** for p < 0.001. Statistical significance for A is determined using the Wilcoxon rank-sum test. The log-rank test for B. Spearman correlation analysis for C. One-way ANOVA for E, F.

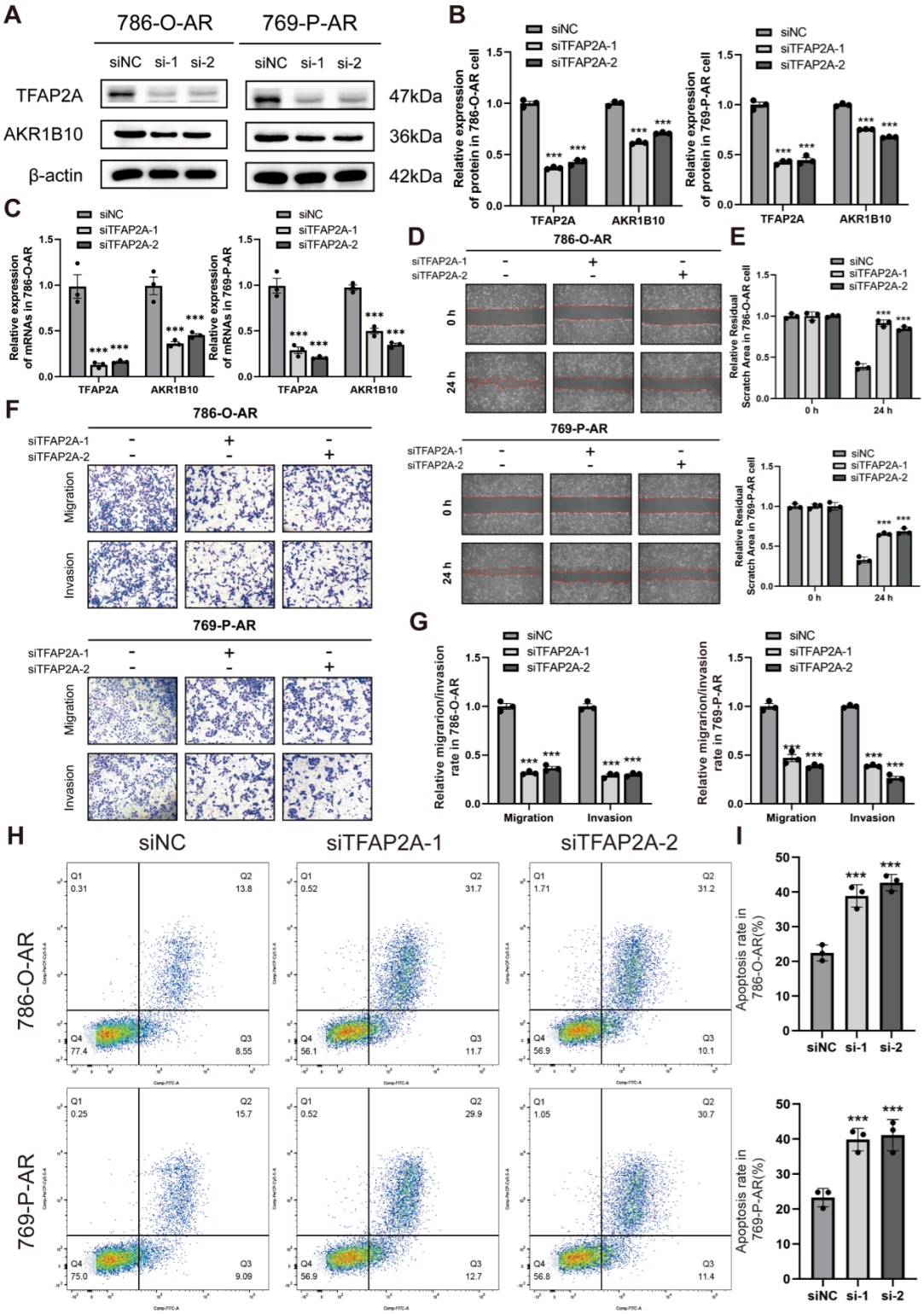


Figure 6

Knockdown of TFAP2A downregulates the expression of AKR1B10 and suppresses the anti-apoptotic, migratory and invasive abilities of ccRCC. A-C The RT-qPCR and Western blot experiments showed the efficiency of TFAP2A knockdown and the changes in the expression level of AKR1B10 at the mRNA and protein levels after shTFAP2A transfection. **D, E**The migratory capacity of 786-O-AR and 769-P-AR cells after knockdown of TFAP2A was assessed using a wound healing assay. **F, G** The migration and invasion capacity of 786-O-AR and 769-P-AR cells after knockdown of TFAP2A was assessed using a transwell cell migration/invasion assay. **H-I** FITC/PI double staining combined with flow cytometry demonstrated that after knockdown of TFAP2A, the anti-apoptotic capabilities of 786-O-AR and 769-P-AR cells were suppressed.

All data in this figure are represented as mean +/- SD (n = 3 per group).

*** for $p < 0.001$. Statistical significance for B, C, E, G and I is determined using one-way ANOVA.

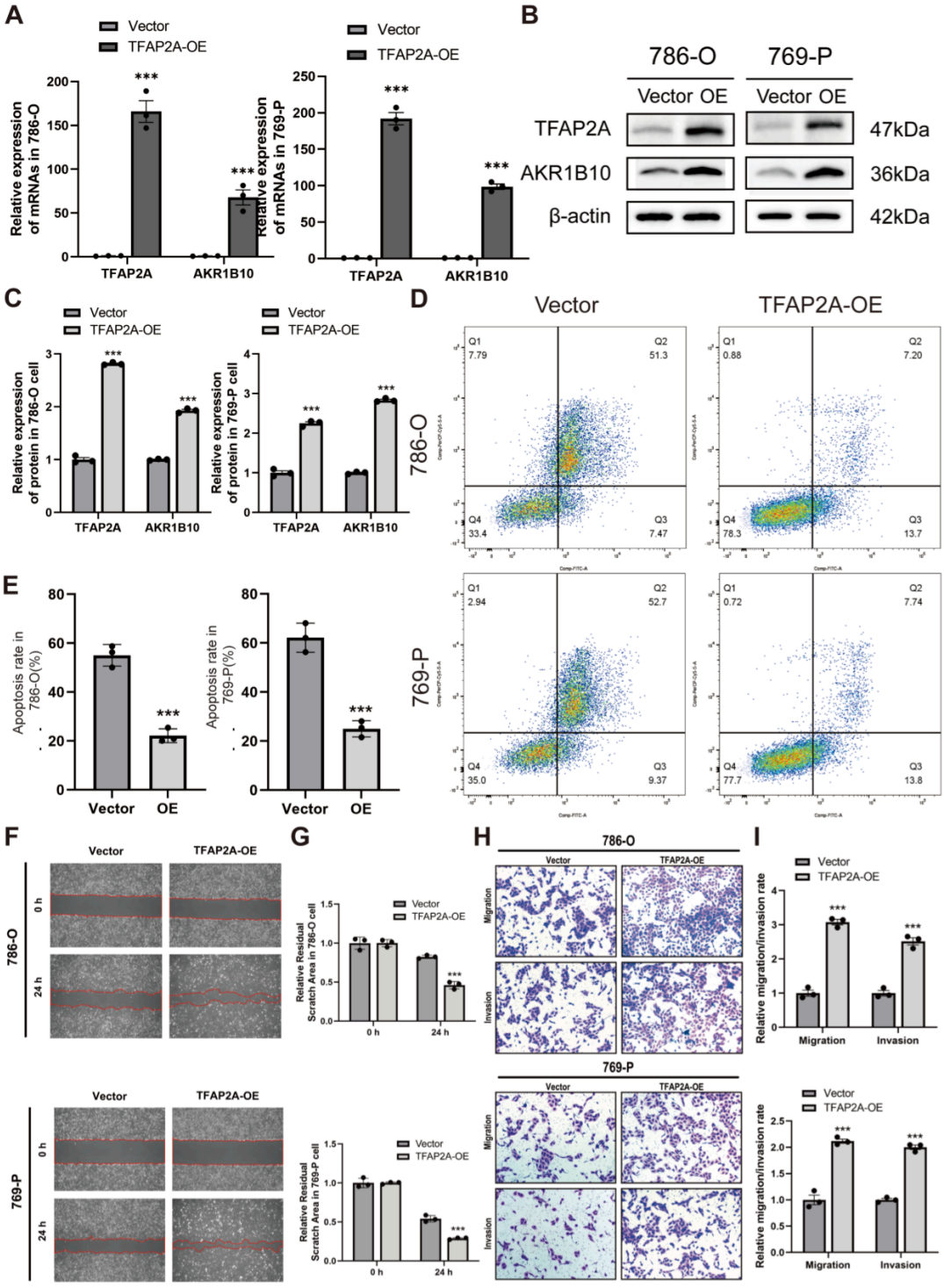


Figure 7

Overexpression of TFAP2A upregulates the expression of AKR1B10 and enhances the anti-apoptotic, migratory and invasive abilities of ccRCC. A-C The RT-qPCR and Western blot experiments showed the efficiency of TFAP2A overexpression and the changes in the expression level of AKR1B10 at the mRNA and protein levels after TFAP2A-OE plasmids transfection. **D, E** FITC/PI double staining combined with flow cytometry demonstrated that after overexpression of TFAP2A, the anti-apoptotic capabilities of 786-

O and 769-P cells were enhanced. **F, G** The migratory capacity of 786-O-AR and 769-P-AR cells after overexpression of TFAP2A was assessed using a wound healing assay. **H, I** The migration/invasion capacity of 786-O-AR and 769-P-AR cells after overexpression of TFAP2A was assessed using a transwell cell migration and invasion assay.

All data in this figure are represented as mean +/- SD (n = 3 per group).

*** for $p < 0.001$. Statistical significance for A, C, E, G and I is determined using one-way ANOVA.

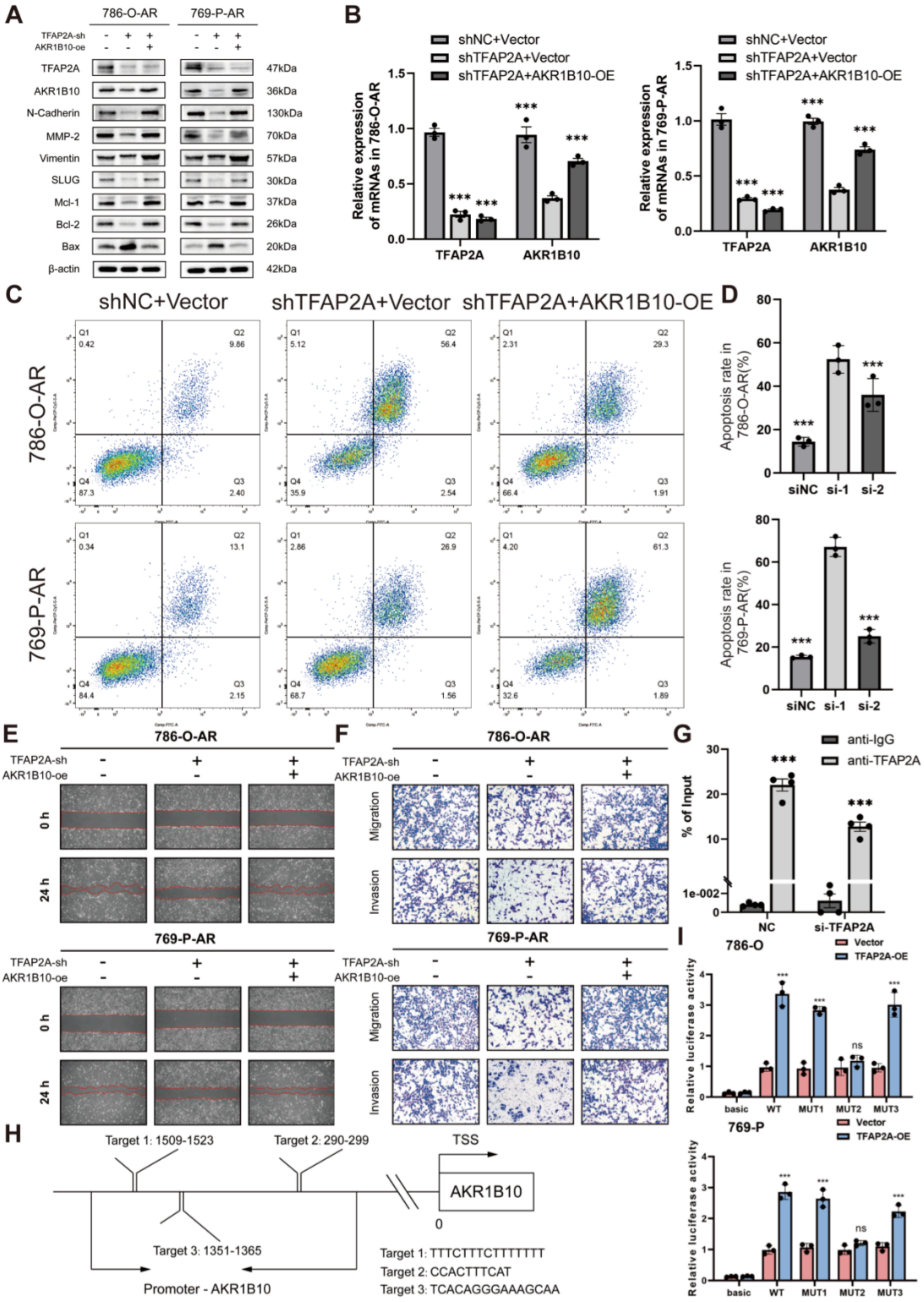


Figure 8

TFAP2A binds to the promoter region of AKR1B10 in ccRCC, thereby mediating downstream biological behaviors. A,B The RT-qPCR and Western blot experiments showed the alterations in the mRNA and protein expression levels of TFAP2A and AKR1B10 after co-transfection with siTFAP2A and AKR1B10-OE in 786-O-AR and 769-P-AR. **C, D** FITC/PI double staining combined with flow cytometry demonstrated that overexpression of AKR1B10 reversed the suppressed anti-apoptosis capacity. **E** Wound healing

assay revealed that overexpression of AKR1B10 restored the attenuated migratory capacity. **F** Transwell cell migration/invasion experiment revealed that overexpression of AKR1B10 restored the attenuated migration and invasion capacity. **G** Chromatin immunoprecipitation combined with quantitative PCR (ChIP-qPCR) revealed that the enrichment level in the AKR1B10 promoter region was decreased in the TFAP2A knockdown group. **H** Information on potential binding sites of TFAP2A and AKR1B10 in the promoter region. **I** Dual-luciferase reporter assays on the binding site of the AKR1B10 promoter in 786-O and 769-P cell lines.

All data in this figure are represented as mean +/- SD (n = 3 per group).

Ns for statistical significance, *** for $p < 0.001$. Statistical significance for B, D, G and I is determined using one-way ANOVA.

Supplementary Files

This is a list of supplementary files associated with this preprint. Click to download.

- Supplementarymaterial.docx